Immunotoxin SS1P is rapidly removed by proximal tubule cells of kidney, whose damage contributes to albumin loss in urine

Xui-Fen Liu[a], Junxia Wei[a], Qi Zhou[a], Bruce A. Molitoris[b,c], Ruben Sandoval[b,c], Hisataka Kobayashi[d], Ryuhei Okada[d], Tadanobu Nagaya[d], Baktiar Karim[e], Donna Butcher[e], and Ira Pastan[a,1]

[a]Laboratory of Molecular Biology, Center for Cancer Research, National Cancer Institute, National Institutes of Health, Bethesda, MD 20892; [b]Department of Medicine, Division of Nephrology, Indiana Center for Biological Microscopy, Indiana University School of Medicine, Indianapolis, IN 46202; [c]Nephrology Research II, Richard L. Roudebush Veterans Affairs Medical Center, Indianapolis, IN 46202; [d]Molecular Imaging Program, National Cancer Institute, Bethesda, MD 20892; and [e]Pathology/Histotechnology Laboratory, Leidos Biomedical Research, Inc., Frederick National Laboratory for Cancer Research, Frederick, MD 21702

Contributed by Ira Pastan, January 20, 2020 (sent for review November 1, 2019; reviewed by Antonio Tito Fojo, Michael G. Rosenblum, and Elad Sharon)

Recombinant immunotoxins (RITs) are chimeric proteins composed of an Fv and a protein toxin being developed for cancer treatment. The Fv brings the toxin to the cancer cell, but most of the RITs do not reach the tumor and are removed by other organs. To identify cells responsible for RIT removal, and the pathway by which RITs reach these cells, we studied SS1P, a 63-kDa RIT that targets mesothelin-expressing tumors and has a short serum half-life. The major organs that remove RIT were identified by live mouse imaging of RIT labeled with FNIR-Z-759. Cells responsible for SS1P removal were identified by immunohistochemistry and intravital two-photon microscopy of kidneys of rats. The primary organ of SS1P removal is kidney followed by liver. In the kidney, SS1P passes through the glomerulus, is taken up by proximal tubular cells, and transferred to lysosomes. In the liver, macrophages are involved in removal. The short half-life of SS1P is due to its very rapid filtration by the kidney followed by degradation in proximal tubular cells of the kidney. In mice treated with SS1P, proximal tubular cells are damaged and albumin in the urine is increased. SS1P uptake by kidney is reduced by coadministration of L-lysine. Our data suggests that L-lysine administration to humans might prevent SS1P-mediated kidney damage, reduce albumin loss in urine, and alleviate capillary leak syndrome.

half-life | proximal tubule | mesothelin | cancer | CLS

Recombinant immunotoxins (RITs) are chimeric proteins being developed for the treatment of cancer (1, 2). We have developed RITs composed of the Fv portion of antibodies fused to a 38-kDa fragment of *Pseudomonas* exotoxin A (PE). The Fv brings the toxin to the cancer cell, and the toxin enters and kills the cell (1, 2). Moxetumomab pasudotox is a RIT that targets CD22, which is expressed on most B cell malignancies, including hairy cell leukemia (3). Moxetumomab pasudotox has produced many complete and durable remissions in patients with chemo-refractory hairy cell leukemia (3). It has been granted Food and Drug Administration (FDA) approval for the treatment of refractory hairy cell leukemia (https://www.fda.gov/vaccines-blood-biologics/compliance-actions-biologics/clinical-investigator-inspection-list-e-k).

Moxetumomab pasudotox and related RITs, like LMB-2, which targets CD25 on T cell malignancies, and SS1P, which targets mesothelin on solid tumors, have a molecular mass of 63 kDa and a short half-life of 15–20 min in the circulation of mice (4, 5). To study the biodistribution of RITs, we have previously labeled LMB-2 with Indium^{111}, injected it into mice, and found that 60% of the LMB-2 was rapidly removed by the kidney and most of the remainder by the liver (6), but the cells contributing to removal in the kidney were not identified. We have now investigated factors responsible for the short 19-min half-life of SS1P. We find that rapid filtration through the glomerulus and subsequent uptake and destruction in proximal tubule cells are responsible.

Results

Our goal was to identify the organs and the cells within those organs that are responsible for removal of SS1P from the blood. SS1P is a 63-kDa protein composed of an anti-mesothelin Fv fused to a 38-kDa fragment of PE (Fig. 1*A*). To identify the organs responsible for the removal of SS1P, we used an imaging method that allows continuous monitoring of uptake (7). SS1P was labeled with FNIR-Z-759, a dye that emits light in the near infrared and can be detected externally by imaging the mice. Fig. 1*B* shows dorsal and ventral images of a tumor-bearing mouse taken at various times after the injection of SS1P-FNIR-Z-759. Because the kidney and tumor are close to the skin on the dorsal side of the mouse, they can be detected on dorsal imaging shown in upper images, whereas the liver is close to the ventral region of the mouse and is detected on ventral imaging. The dorsal images show rapid uptake by kidney and slower uptake by the tumor. A signal was detected in the kidney immediately after injection, increased to a maximum at 2 h, and persisted for many hours. Uptake by the tumor was slow, very weak at 15 min, and did not become strong for several hours (Fig. 1*B*). The ventral image shows rapid uptake by the liver. There is also some signal in the bladder, which is due to removal of the dye from the protein, as analysis of the urine failed to show significant amounts of RIT. Usually the flourscence remained long after the protein was degraded.

Significance

This paper shows that the major pathway of degradation of immunotoxins in mice is rapid filtration through the glomerulus of the kidney and degradation by proximal tubular cells. It also shows that SS1P treatment damages proximal tubular cells and enhances loss of albumin in the urine, which can contribute to capillary leak syndrome, a major side effect of immunotoxin therapy. Because lysine administration diminishes kidney uptake of SS1P, it could also protect against SS1P-induced capillary leak syndrome.

Author contributions: B.A.M., H.K., and I.P. designed research; X.-F.L., J.W., Q.Z., B.A.M., R.S., H.K., R.O., T.N., B.K., and D.B. performed research; X.-F.L., B.A.M., R.S., H.K., R.O., T.N., and I.P. analyzed data; and X.-F.L. and I.P. wrote the paper.

Reviewers: A.T.F., Columbia University Medical Center; M.G.R., University of Texas MD Anderson Cancer Center; and E.S., National Cancer Institute.

Competing interest statement: I.P. is the inventor on many immunotoxin patents that have all been assigned to NIH. I.P. and A.T.F. are coauthors on a 2016 article. They did not collaborate directly on the work. X.-F.L., J.W., Q.Z., I.P., and E.S. are affiliated with the National Cancer Institute.

[1]To whom correspondence may be addressed. Email: pastani@mail.nih.gov.

First published March 2, 2020.

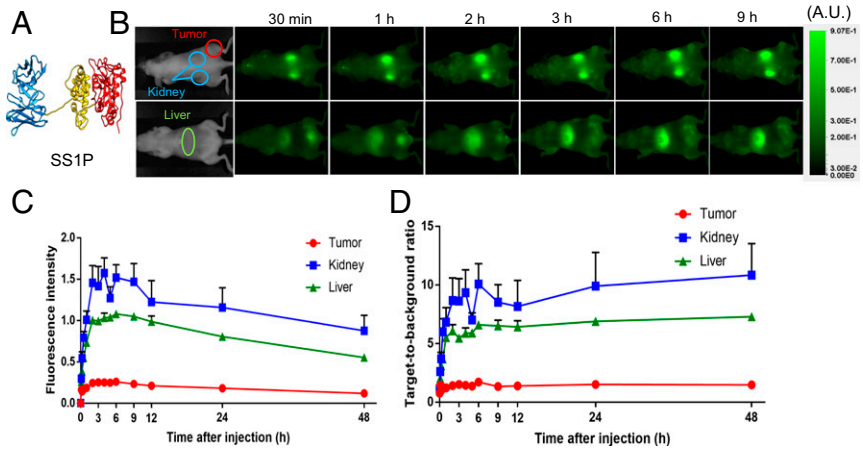

Fig. 1. (*A*) Ribbon diagram of immunotoxin SS1P. Fv is in blue, domain II is in yellow, and domain III of PE is in red. The structural model was generated by using UCSF Chimera. (*B*) Uptake of SS1P by kidney, liver, and tumor in BALB/c mice. *C* and *D* are quantification of uptake by kidney, liver, and A431/H9 tumor. The target-to-background ratio indicates the fluorescence subtracted from the background.

The fluorescence images were quantified and the amount in the kidney, liver, and tumor are shown in Fig. 1 *B* and *C*. The kidney accumulated more SS1P than the liver. Kidney and liver uptake peaked by 1 h, whereas the uptake by tumor increased over several hours. Accumulation of fluorescence reflects an equilibrium between RIT uptake and degradation and/or removal of the fluorescent label, which is excreted in the urine.

To determine the state of SS1P in the kidney and liver, we performed Western blots shown in Fig. 2*A*. Mice were injected with SS1P and at 5, 15, 30, and 60 min, kidneys and livers were removed, extracts prepared, and proteins analyzed by SDS/PAGE and Western blotting. Fig. 2 shows that 5 and 15 min after injection, a large amount of intact SS1P was detected in the kidney, but by 1 h, it was degraded, although the fluor remained in the kidney for many hours (Fig. 1). Fig. 2 also shows that degradation by liver is rapid with very little SS1P detectable at 30 and 60 min.

SS1P Localization in Kidney and Liver. We used immunohistochemistry to determine which cells in the kidney contained SS1P. To detect the protein, we used the same anti-toxin antibody used for Western blotting. Fig. 2*B* shows low power (*a*, *c*) and high-power images (*b*, *d*) of kidney and liver harvested 15 min after intravenous (i.v.) injection of SS1P. In the kidney (*a* and *b*), there is a strong signal in proximal tubular cells in the cortical region but very little signal in distal tubules or glomeruli. Fig. 2*B* (*c* and *d*) shows sections of liver 15 min after SS1P injection. There is multifocal RIT-positive staining (brown) in the sinusoidal spaces, predominantly in midzonal and periportal areas. The high-power view (*d*) shows staining of cells lining sinusoids, which could be Kupffer cells or endothelial cells or both.

Intravital Microscopy of SS1P in Mice. To confirm the identity of the cells in the kidney accumulating SS1P and to determine the nature of the vesicles that contained SS1P, Munich Wistar Frömter rats were given an i.p. injection of 10-kDa Cascade Blue dextran (blue) to prelabel the lysosomes (8). Sixteen hours later, a 75-μg dose of TR-SS1P was administered i.v. Fig. 3*A* shows a cross-section of outer cortical proximal tubules (PTs) taken 10 min after infusion of TR-SS1P. The majority of the internalized TR-SS1P (red) is seen in small endocytic vesicles at and below the apical membrane (arrow). At this time point, the blue-labeled lysosomes (arrowhead) are essentially free of any TR-SS1P and the two colors are separated from each other. Fig. 3*B* shows the same rat 24 h after the initial dose of TR-SS1P. Here, the vast majority of the TR-SS1P has accumulated within the lysosomal pool and the previously distinct separate pools are now merged to produce a magenta color.

Glomerular Sieving Coefficients. We used two-photon microscopy to measure the concentration of SS1P in Bowman's space and in proximal tubules and calculated Glomerular sieving coefficients (GSCs) (9, 10). The data in Table 1 shows the GSCs measured in these experiments compare them with values for albumin and FITC Dextran previously determined. The GSC for albumin is 0.015 and

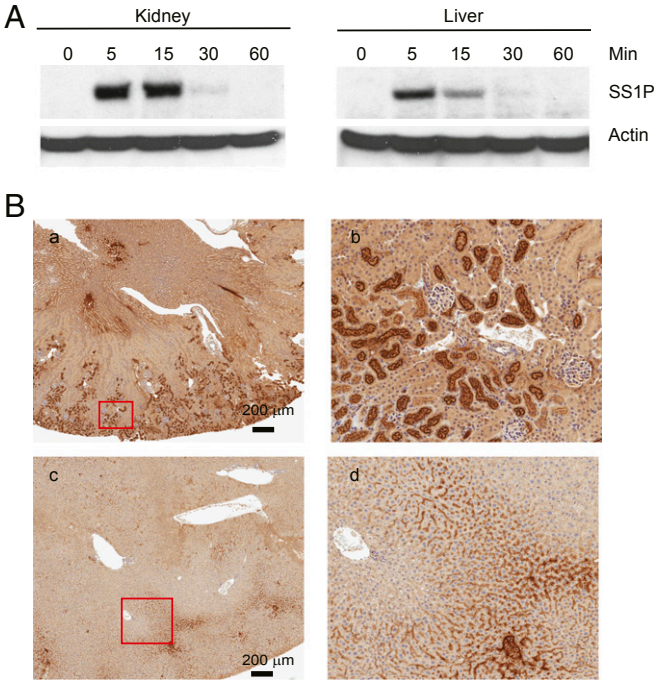

Fig. 2. Immunotoxins in kidney and liver. (*A*) Western blot analysis of SS1P stability: Nude mice were injected with 30 μg of SS1P, and at indicated times, the kidney and liver were removed. Protein lysates were then analyzed by Western blot with anti-PE38. Actin was blotted as loading control. (*B*) Localization of SS1P in kidney and liver. Thirty micrograms of SS1P was injected in nude mice i.v., kidney (*a* and *b*) and liver (*c* and *d*) were removed at 15 min. The kidney and liver sections were immunohistochemically stained with anti-PE38. *b* and *d* are further magnification of the corresponding red box from *a* and *c*.

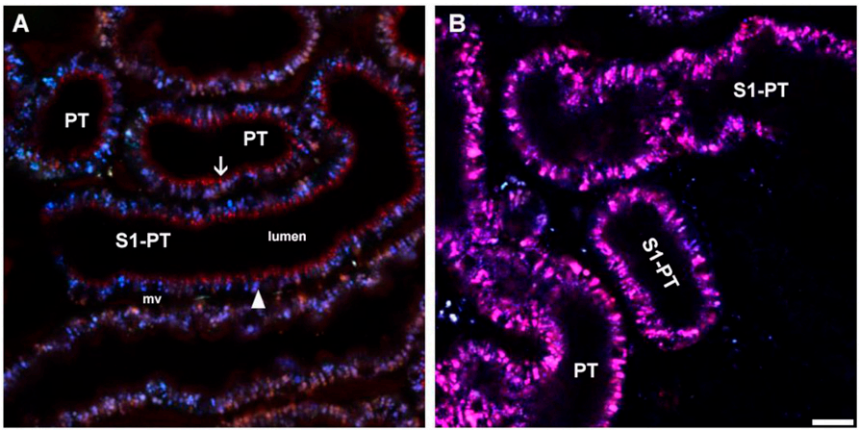

Fig. 3. Localization of SS1P in kidneys of living rats by two-photon microscopy. Munich Wistar Frömter rats were given an i.p. injection of 10-kDa Cascade Blue dextran (blue) to prelabel the lysosomes 16 h earlier. The following day, a 750-μg dose of TR-SS1P was administered i.v. *A* shows a cross-section of outer cortical proximal tubules (PTs) taken 10 min after infusion of TR-SS1P. *B* shows the same rat 24 h after the initial dose of TR-SS1P. (Scale bar: 20 μm.) mv, microvascular space; S1-Pt, the first or S1 portion of the proximal tubule.

that for SS1P is 0.108. The 0.108 value indicates that SS1P is filtered much more rapidly than serum albumin, and this increased filtration rate can account for its rapid removal by the kidney.

Lysine Reduces Kidney Accumulation of SS1P. It has been known for many years that the administration of large amounts of lysine can prevent uptake of small proteins by kidney proximal tubule cells (11), and consequently an infusion of basic amino acids is now used clinically to protect the kidney from radiopharmaceuticals such as Lutetium Lu-177 Dotatate (12). To determine if Lysine infusion would reduce immunotoxin uptake by kidney without affecting tumor uptake, five mice bearing A431/H9 tumors received phosphate buffered saline (PBS) and five received L-lysine (50 mg/200 μL in PBS) intraperitoneally 2 min before an i.v. dose of SS1P-FNIR-Z-759. To assess the effect of lysine on the biodistribution of SS1P, serial dorsal and ventral 800-nm fluorescence images were obtained before and at serial times after injection. Fig. 4*A* shows images illustrating that the signal in the kidney area of the PBS group rose rapidly and remained elevated for many hours. The signal in the group receiving L-lysine rose more slowly and remained below the control group at all times. Fig. 4*B* shows quantification of this data using early time points. There was a significant decrease in uptake by kidney ($P < 0.01$). There was no significant effect of L-lysine on tumor uptake of SS1P (Fig. 4*C*).

Effect of SS1P on PTC Cell Morphology and Function. To determine if accumulation of SS1P in the kidney was accompanied by damage to tubular cells, mice were injected SS1P and kidneys were harvested 24 h later, fixed, sectioned, and the sections stained with hematoxylin and eosin (H&E) and periodic acid-Schiff (PAS). The H&E images in Fig. 5 *A* and *B* show degeneration in the epithelial cells lining tubules (green arrows). The PAS images show loss of the PAS-positive reaction in the brush border region of these cells.

Finally, to determine if proximal tubule cells (PTC) damage is associated with increase in albumin in the urine, mice were treated with SS1P and urine collected 24 h later. The data in Fig. 5*C* shows that urine albumin is elevated in mice receiving 0.5 or 0.75 mg/kg SS1P. The urine albumin levels in untreated mice ranged from 16 to 30 μg/mL. Treatment with 0.5 mg or 0.75 mg/kg of SS1P raised the level to 326 and 980 μg/mL, respectively.

Discussion

Antibody-based therapeutics that contain drug or toxin moieties designed to kill cancer cells are injected i.v. and depend on the circulatory system to deliver them to cancer cells. Unfortunately, only a small portion of these agents reach the cancer cells due to rapid uptake and metabolism by normal organs. In the current study, we have used a variety of approaches to determine which organs, and more specifically, which cells in these organs, participate in RIT removal from the blood and in their destruction. We have studied SS1P, a member of a class of RITs that has been in clinical use for over 10 y. Another member of this class, Moxetumomab pasudotox, was recently FDA approved for treating drug-resistant leukemia in humans. The findings with SS1P are relevant to Moxetumomab pasudotox and other class members like LMB-2 (2, 4).

We find that after uptake by kidney, SS1P is rapidly degraded (Fig. 2*A*). Immunohistochemistry studies show that SS1P is located in PTCs (Fig. 2*B*), and analysis of its location in living rats by intravital two-photon microscopy show that in the PTCs, SS1P is found initially in endosomes and later moves to lysosomes (Fig. 3). Because SS1P is rapidly degraded in the kidney, we assume degradation begins in endosomes shortly after internalization.

The cartoon in Fig. 6 summarizes the events in PTCs in the kidney that occur after SS1P infusion. SS1P is filtered rapidly through the glomerulus and enters lumen of the proximal tubule, where it binds to megalin/cubilin and is endocytosed and degraded by PTCs. Megalin and cubilin have been shown to bind many different proteins that pass through the glomerulus and are present in proximal tubules (13). Albumin is also filtered by PTCs, binds to megalin/cubilin, is taken up by PTCs, undergoes transcytosis, and is released into the extracellular space for recycling. PTCs are damaged by SS1P and have a decreased ability to absorb or transcytose albumin, leading to more albumin in the urine. Lysine competes with SS1P for binding to megalin/cubilin, and cells are protected from cytotoxic effect of SS1P.

Table 1. Glomerular sieving coefficients

Compound	Molecular mass, kDa	GSC	Half-life
Albumin (human)	66.3	0.015 ± 0.001	19 d
FITC Dextran	69.7	0.019 ± 0.002	Not determined
SS1P	63	0.108 ± 0.036	19 min

GSC, glomerular sieving coefficients.

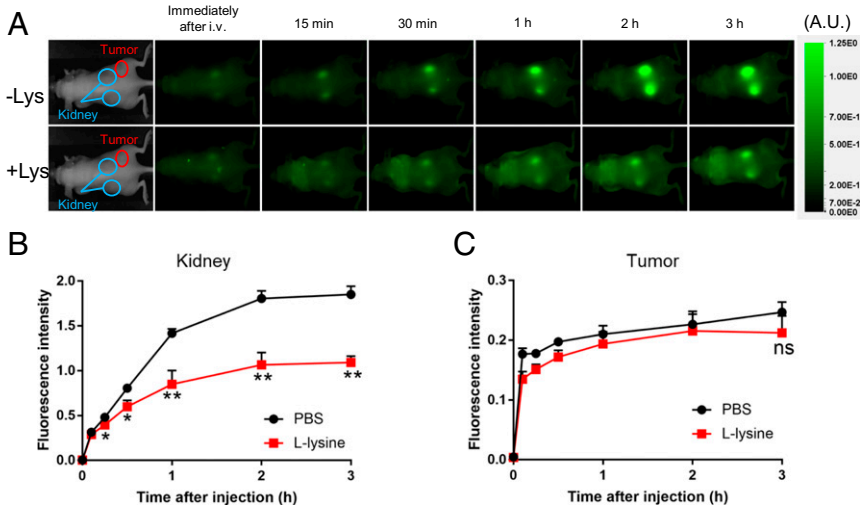

Fig. 4. Uptake of SS1P by kidney was reduced by lysine. (*A*) Mice were injected with either 200 μL of PBS (-Lys) or L-lysine (50 mg/200 μL) i.p. Two minutes later, 25 μg of SS1P-FNIR-Z-759 was i.v. injected and imaged at indicated times. (*B* and *C*) Quantification of kidney fluorescence signals were normalized by target-to-background ratio, calculated as (fluorescence intensity of target)/(fluorescence intensity of background). The mouse images in the *Left* panels are from our archives and are inserted to indicate regions that are imaged.

We also measured the sieving coefficient of SS1P, which indicates how efficiently SS1P passes through the glomerulus into the lumen of the proximal tubule, and determined a coefficient of 0.108 indicating SS1P is filtered much more rapidly than serum albumin, although they have similar molecular masses. Albumin (pI 4.9) is more acidic that SS1P (pI 5.5), and this difference may contribute to the difference.

One of the major side effects of RIT therapy is capillary leak syndrome (CLS), which is characterized by weight gain, edema, and hypoalbuminemia (1, 14). The mechanism of CLS is poorly

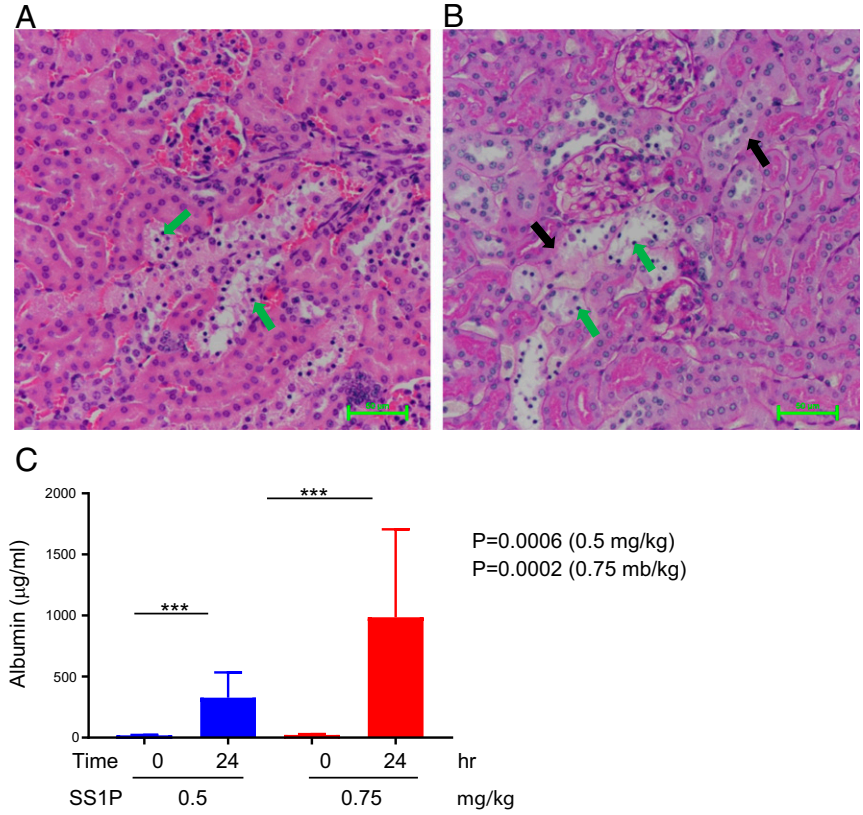

Fig. 5. SS1P-damaged kidney tubular and increased albumin in the urine. Fifty micrograms of SS1P was injected i.v., and mouse kidneys were removed after 24 h. (*A*) Section of H&E stain of kidney showing widening tubular lumen, sloughed epithelial cells lining tubules, pyknotic nuclei/apoptotic changes (green arrows), and loss of brush border. (*B*) PAS staining showing loss of PAS-positive reaction in the brush border region, damaged basement membrane (black arrows), and pyknotic nuclei (green arrows). (*C*) Albumin in urine increased after SS1P administration. Albumin levels were measured before the 0.5 or 0.75 mg/mL SS1P injection (0 h) or 24 h after injection. $n = 3$ mice each group.

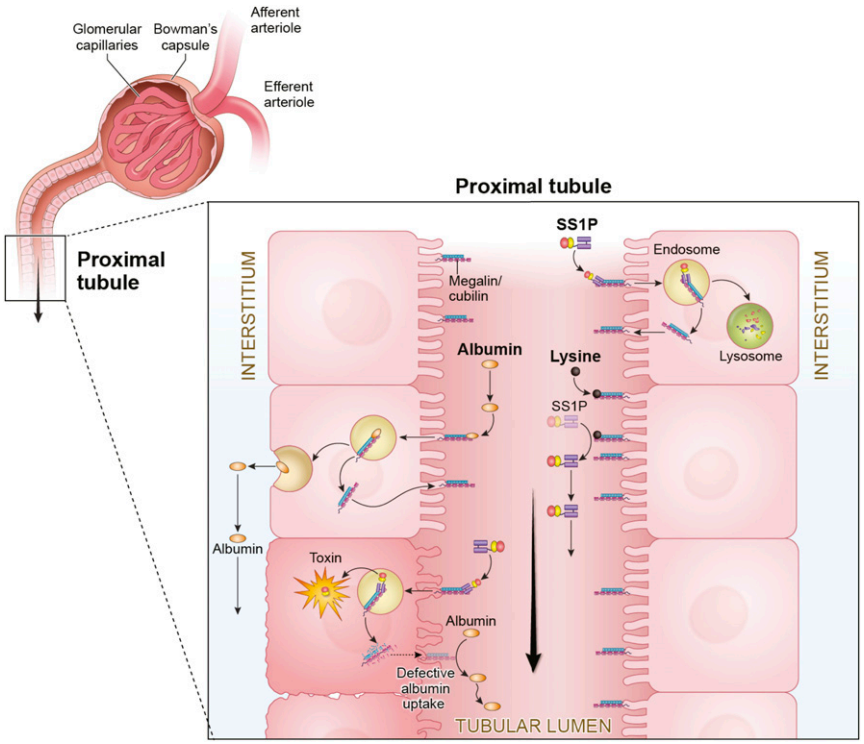

Fig. 6. Illustration of SS1P in the kidney tubule. SS1P is filtered through glomerular and accumulated in the proximal tubule. It can be uptake by the tubule cells through endosome and degraded in the lysosome. Some portion of albumin is also filtered by PTCs, binds to megalin/cubilin, and undergoes transcytosis. PTCs are damaged by SS1P and have a decreased ability to absorb or transcytose albumin leading to more albumin in the urine. Lysine can compete with SS1P and reduced SS1P uptake.

understood. CLS has been proposed to be due to several factors, one of which is direct damage to endothelial cells resulting in fluid loss into tissues (9, 15, 16). While direct endothelial cell damage may occur with antibody-toxin conjugates that have a high molecular mass and a long circulation time, it may not entirely explain CLS caused by RITs that are rapidly removed from the circulation. The current study shows that large amounts of RITs are taken up by PTCs, that SS1P has the capacity to damage PTCs as shown in Fig. 5, and that SS1P also increases albumin in the urine. We propose that PTCs that are injured by SS1P have a reduced ability to reabsorb and/or transcytosis albumin from the primary urine. This, in turn, could cause reduced serum albumin levels (10, 17), resulting in edema and volume retention. In addition, PTCs have a major role in modulating the response to angiotensin, which through its action on aldosterone is a major regulator of sodium homeostasis (18). An increase in sodium reabsorption caused by angiotensin released by the kidney could lead to sodium retention and edema. We have also found that administration of large amounts of lysine to mice decreases SS1P uptake by kidneys (Fig. 4). It is possible that lysine, by blocking uptake of SS1P and other RITs by proximal tubular cells, could diminish CLS and allow larger amounts of RITs to be safely given to patients. A clinical trial to test this hypothesis is being planned.

Materials and Methods

Reagents. SS1P was manufactured by Advanced Bioscience Laboratories Inc. The kit to measure mouse albumin was purchased from Molecular Innovation.

Protein Labeling. SS1P was labeled with Alexa 647, Oregon Green-488, or Texas Red following the manufacturer's instructions (Thermo Scientific). Conjugation of dye FNIR-Z-759 with SS1P was performed according to previous reports (7). In brief SS1P was incubated with fourfold molar amount of FNIR-Z-759 in 0.1 mol/L Na_2HPO_4 (pH 8.5) at room temperature for 1 h. The mixture was purified with a Sephadex G25 column (PD-10; GE Healthcare). The protein concentration was determined with the Coomassie Plus protein assay kit (Thermo Fisher Scientific). The concentration of dye was measured by absorption at 759 nm to confirm the number of fluorophore molecules conjugated to each RIT. The synthesis was controlled so that an average of two dye molecules were bound to a single protein. We performed SDS/PAGE as a quality control for the conjugate as previously reported (7).

In Vivo Fluorescence Imaging. In vivo fluorescence images were obtained with a Pearl Imager (LI-COR Bioscience) after i.v. injection of 25 μg of labeled SS1P. Mice were imaged before and immediately after injection, at 15 and 30 min, and 1, 2, 3, 4, 5, 6, and 9 h after injection. Equal sized regions of interest (ROIs) were manually drawn on each target, and fluorescence intensity at 800 nm was measured. When comparing fluorescence, Pearl Cam software (LI-COR Biosciences) was used for calculating the average fluorescence intensity of each target ROI. ROIs were also placed in the adjacent nontumor region (e.g., a symmetrical region to the left of the tumor) and fluorescence measured as previously. Target-to-background ratio (TBR) was calculated using following formula: TBR = (mean target intensity)/(mean background intensity).

Western Blot Analysis. SS1P was injected into mice i.v. At the times indicated in the figures, the mice were killed, the livers and kidneys were removed, and frozen on dry ice. The tissues were lysed in lysis buffer (50 mM Tris·HCl, 150 mM NaCl, 5 mM EDTA) with 1% Nonidet P-40, 5 μg/mL leupeptin, 5 μg/mL aprotinin, 10 μM phenylmethylsulfonyl fluoride and homogenized on ice. After high-speed centrifugation, supernatants were analyzed by SDS/PAGE, transferred to a polyvinylidene fluoride membrane, and subjected to Western blot analysis with anti-PE antibody.

Immunohistochemical Study. Thirty micrograms of SS1P was injected i.v. into each mouse. After 15 or 45 min, the liver or kidney was removed and put in 10% NBF fixation for 96 h, then transferred into 70% ethanol. Five-micrometer-thick sections from formalin-fixed paraffin-embedded kidney or liver were mounted on charged slides and double stained on Leica Biosystems' BondRX auto-stainer. Following EDTA antigen retrieval, tissues were blocked for endogenous peroxidase with 3% H_2O_2. Anti-PE38 primary

antibody at 20 μg/mL was applied to tissues for 30 min. Immunohistochemistry followed with the Bond Polymer Refine Red Detection Kit (Leica Biosystems DS9390), with omission of the Post Primary Reagent and hematoxylin. Tissues were then blocked for endogenous biotin with the Avidin/Biotin Blocking Kit (Vector Laboratories). Immunohistochemistry continued with the Bond Intense R Detection Kit (Leica Biosystems DS9263), with omission of the peroxidase blocking reagent. Slides were removed from the auto-stainer, dehydrated through graded ethanol, cleared in xylene, and put on coverslips with Tissue-Tek Glas (Sakura) mounting medium.

Two-Photon Microscopy. Imaging was conducted using an Olympus FV1000 microscope adapted for two-photon microscopy with high-sensitivity gallium arsenide nondescanned 12-bit detectors with animal preparations, as described previously (19). Rats were anesthetized with inactin (130 mg/mL, at a dose of ∼12 mg/100 g body weight). A jugular venous line was used to introduce fluorescent compounds. Mice were anesthetized using isoflurane, 5% induction 1.5–2.0% maintenance at 0.5 L of O_2/min.

Quantitative Process of GSCs. GSCs were determined as described by Sandoval et al. (19). Briefly, images of the glomerulus were taken prior to infusion of fluorescent conjugates to determine background levels within the capillary loops and Bowman's Space. These background values were then subtracted from the corresponding intensity values to generate background corrected values. The Bowman's space intensities were divided by the capillary loop plasma intensities to determine GSCs. Plasma intensity values for fluorescent conjugates were determined by following the identical region within a plane of focus. Quantitation of images was performed using Metamorph v 6.1 (Molecular Devices). Graphs and mathematical summaries were generated using Microsoft Excel.

Urine Collection and Albumin Measurement. To measure albumin in the urine, urine was collected before injection of each mice by holding the mouse over the collection device tube and lightly stroking the belly of the animal. SS1P was injected i.v., and 22 h later the bladder was emptied by massaging the bellies of mice, then the urine was collected 24 h after SS1P injection. Albumin level in the urine was measured by using mouse albumin antigen ELISA kit (catalog number MSAKT).

Female NSG mice were obtained from National Cancer Institute Frederick facility. Munich Wistar Frömter rats (9–12 wk old) were derived from a colony generously provided by Roland Blantz (University of California, San Diego, CA). All rats and mice were given water and food ad libitum throughout the study. All experiments followed the NIH *Guide for the Care and Use of Laboratory Animals* guidelines (20) and were approved by the Animal Care of the National Cancer Institute and Use Committee at the Indiana University School of Medicine.

Data Availability. All relevant data are included in the manuscript; associated protocols and materials are available upon request.

ACKNOWLEDGMENTS. This research was supported by the Intramural Research Program of the NIH, National Cancer Institute, Center for Cancer Research, NIH P-30 O'Brien application Grant P30-DK07931 (to B.A.M.).

1. C. Alewine, R. Hassan, I. Pastan, Advances in anticancer immunotoxin therapy. *Oncologist* **20**, 176–185 (2015).
2. I. Pastan, R. Hassan, D. J. Fitzgerald, R. J. Kreitman, Immunotoxin therapy of cancer. *Nat. Rev. Cancer* **6**, 559–565 (2006).
3. R. J. Kreitman *et al*., Phase I trial of anti-CD22 recombinant immunotoxin moxetumomab pasudotox (CAT-8015 or HA22) in patients with hairy cell leukemia. *J. Clin. Oncol.* **30**, 1822–1828 (2012).
4. M. Onda *et al*., Lowering the isoelectric point of the Fv portion of recombinant immunotoxins leads to decreased nonspecific animal toxicity without affecting antitumor activity. *Cancer Res.* **61**, 5070–5077 (2001).
5. J. E. Weldon *et al*., A recombinant immunotoxin against the tumor-associated antigen mesothelin reengineered for high activity, low off-target toxicity, and reduced antigenicity. *Mol. Cancer Ther.* **12**, 48–57 (2013).
6. H. Kobayashi *et al*., Pharmacokinetics of 111In- and 125I-labeled antiTac single-chain Fv recombinant immunotoxin. *J. Nucl. Med.* **41**, 755–762 (2000).
7. T. Nagaya *et al*. Molecularly targeted cancer combination therapy with near-infrared photoimmunotherapy and near-infrared photorelease with duocarmycin–antibody conjugate. *Mol. Cancer Ther.* **17**, 661–670 (2018).
8. N. B. Yapici *et al*., Highly stable and sensitive fluorescent probes (LysoProbes) for lysosomal labeling and tracking. *Sci. Rep.* **5**, 8576 (2015).
9. Y. Cao *et al*., Design optimization and characterization of Her2/neu-targeted immunotoxins: Comparative in vitro and in vivo efficacy studies. *Oncogene* **33**, 429–439 (2014).
10. L. M. Russo *et al*., The normal kidney filters nephrotic levels of albumin retrieved by proximal tubule cells: Retrieval is disrupted in nephrotic states. *Kidney Int.* **71**, 504–513 (2007).
11. H. Kobayashi *et al*., L-lysine effectively blocks renal uptake of ^{125}I- or ^{99m}Tc-labeled anti-Tac disulfide-stabilized Fv fragment. *Cancer Res.* **56**, 3788–3795 (1996).
12. B. L. Kam *et al*., Lutetium-labelled peptides for therapy of neuroendocrine tumours. *Eur. J. Nucl. Med. Mol. Imaging* **39** (suppl. 1), S103–S112 (2012).
13. R. Nielsen, E. I. Christensen, H. Birn, Megalin and cubilin in proximal tubule protein reabsorption: From experimental models to human disease. *Kidney Int.* **89**, 58–67 (2016).
14. G. H. Jeong *et al*., Incidence of capillary leak syndrome as an adverse effect of drugs in cancer patients: A systematic review and meta-analysis. *J. Clin. Med.* **8**, E143 (2019).
15. R. Baluna, E. S. Vitetta, Vascular leak syndrome: A side effect of immunotherapy. *Immunopharmacology* **37**, 117–132 (1997).
16. V. Bachanova *et al*., Phase I study of a bispecific ligand-directed toxin targeting CD22 and CD19 (DT2219) for refractory B-cell malignancies. *Clin. Cancer Res.* **21**, 1267–1272 (2015).
17. M. C. Wagner *et al*., Proximal tubules have the capacity to regulate uptake of albumin. *J. Am. Soc. Nephrol.* **27**, 482–494 (2016).
18. C. Caruso-Neves, S. H. Kwon, W. B. Guggino, Albumin endocytosis in proximal tubule cells is modulated by angiotensin II through an AT2 receptor-mediated protein kinase B activation. *Proc. Natl. Acad. Sci. U.S.A.* **102**, 17513–17518 (2005).
19. R. M. Sandoval, B. A. Molitoris, Quantifying glomerular permeability of fluorescent macromolecules using 2-photon microscopy in Munich Wistar rats. *J. Vis. Exp.*, 10.3791/50052 (2013).
20. National Research Council, *Guide for the Care and Use of Laboratory Animals* (National Academies Press, Washington, DC, ed. 8, 2011).